JPEDAV (2006) 27:614-621
DOI: 10.1361/154770306X153639
1547-7037/$19.00 ©ASM International

Irradiation-Enhanced Interdiffusion in the Diffusion Zone of U-Mo Dispersion Fuel in Al

Yeon Soo Kim, G.L. Hofman, Ho Jin Ryu, and S.L. Hayes

(Submitted March 22, 2006; in revised form May 30, 2006)

Uranium-molybdenum (U-Mo) alloy fuel particles dispersed in an aluminum (Al) matrix, designated as U-Mo/Al dispersion fuel, is in the development stage in the worldwide RERTR (Reduced Enrichment for Research and Test Reactors) program. The main issue in developing U-Mo/Al dispersion fuel is the diffusion reaction occurring at the interface between the fuel particles and matrix. To accurately analyze fuel performance, a model to predict the diffusion kinetics is necessary. For this purpose, the authors developed a diffusion layer growth rate correlation for out-of-pile annealing tests and a similar correlation for in-reactor tests. The correlation for in-reactor tests is considerably different from that of out-of-pile tests because it contains factors that amplify diffusion kinetics by fission damage in the diffusion reaction zone. This irradiation enhancement was formulated by a combination of the fission rate in the fuel and fission fragment damage distribution in the diffusion reaction zone. Using a computer code, fission damage factors were obtained as a function of diffusion reaction layer thickness and composition. The model correlation was established and fitted to the in-reactor data. As a result of this data fitting, the interaction layer growth rate is found to be proportional to the square root of the fission fragment damage rate and to have a temperature dependence characterized by the effective activation energy of 46 to 76 kJ/mole, which is smaller by a factor of 4 to 7 than that of out-of-pile tests.

Keywords fission damage, interaction layer growth correlation, irradiation-enhanced interdiffusion, RERTR nuclear fuel, U-Mo dispersion in Al

1. Introduction

Dispersion fuels containing uranium-molybdenum (U-Mo) alloy particles in an aluminum (Al) matrix are being developed for research and test reactors in the RERTR (Reduced Enrichment for Research and Test Reactors) program. The main issue in the process of developing dispersion fuel is the formation of a U-Mo-Al interaction layer occurring at the interface between the fuel and matrix as a result of interdiffusion of constituents of fuel and Al. The major disadvantage of this interaction layer (IL) growth is a significant reduction in thermal conductivity of the dispersion fuel. This causes a positive feedback mechanism to increase the fuel temperature, which promotes the fuel-matrix diffusion reaction to proceed faster.

The diffusion-zone thickness of U-Mo/Al dispersion fuel is usually described by an Arrhenius-type equation for out-of-reactor data typically obtained at high temperatures around 550 °C. Although there are diffusion couple test data of U-Mo against Al, in the current study, the authors used only data from annealing tests of dispersion fuel fabricated with gamma-stabilized U-Mo spherical particles in an Al matrix that are identical to the fuel used in the irradiation tests.[1] As a result, a correlation was developed for diffusion-zone thickness from annealing tests of dispersion fuel.

The IL growth rate of the irradiation tests are many orders of magnitude higher than the predictions by the out-of-reactor correlation at reactor operation temperatures of ~150 °C. This is due to irradiation-enhanced diffusion caused by fission fragment damage in the interdiffusion zone. Irradiation enhancement was modeled as a combination of the fission rate in the fuel and fission fragment damage in the IL. For this purpose, data measured from various in-reactor tests were used, primarily from RERTR tests at ANL and KOMO tests at KAERI. For irradiation tests, dispersion fuel with the same as-fabricated conditions as the out-of-pile data was used. In this paper, the methods to correlate the factors involved in irradiation enhancement and the correlation for IL thickness of irradiated U-Mo/Al dispersion fuel are described.

2. Posttest Fuel Characterization

An example of the cross section of a typical irradiated fuel plate used to obtain interdiffusion layer thickness mea-

This article was presented at the Multicomponent-Multiphase Diffusion Symposium in Honor of Mysore A. Dayananda, which was held during TMS 2006, 135th Annual Meeting and Exhibition, March 12-16, 2006, in San Antonio, TX. The symposium was organized by Yongho Sohn of University of Central Florida, Carelyn E. Campbell of National Institute of Standards and Technology, Richard D. Sisson, Jr., of Worcester Polytechnic Institute, and John E. Morral of Ohio State University.

Yeon Soo Kim and **G.L. Hofman,** Argonne National Laboratory, 9700 South Cass Ave., Argonne, IL 60439; **Ho Jin Ryu,** Argonne National Laboratory, 9700 South Cass Ave., Argonne, IL 60439 and Korea Atomic Energy Research Institute, 150 Deokjin-dong, Yuseong-gu, Daejeon 305-353, Republic of Korea; and **S.L. Hayes,** Idaho National Laboratory, P.O. Box 1625, Idaho Falls, ID 83415-6188. Contact e-mail: yskim@anl.gov.

surements is shown in Fig. 1. These fuels are made of spherical U-Mo fuel particles dispersed in an Al matrix and denoted as U-Mo/Al. Throughout this paper, U-Mo fuel is an alloy of 90 wt.% U and 10 wt.% Mo (i.e., 80 at.% U and 20 at.% Mo). Due to the high thermal conductivity of the metallic dispersion fuel as well as the thin plate-type fuel geometry (1.4 mm in thickness), the fuel temperature was practically uniform across the fuel cross section. Fission density was also considered to be uniform because neutron flux depression is negligible. In Fig. 1, the black circles are U-Mo fuel particles, the gray girth on the fuel particles is the diffusion reaction zone, and the brightest area surrounding the dispersed particles is the unreacted Al matrix. The diffusion reaction zone normally grows fairly uniformly on the fuel particles.

Scanning electron microscope (SEM) images of U-Mo/Al dispersion fuels from an annealing test and an irradiation test, respectively, are juxtaposed in Fig. 2.[1,2] As shown in Fig. 2(a), the high-temperature annealing test resulted in three distinct layers formed between U-Mo and Al: a shallow outer layer, a thick gray intermediate layer, and a brighter inner layer. An electron probe microanalysis (EPMA) result revealed that the three diffusion reaction layers were different in overall composition. The layer toward the Al matrix had the highest Al composition while the layer toward U-Mo had the lowest Al composition. The individual layers are composed of two phases, with a morphology too fine to be resolved with EPMA. The brightest phase at the center of the spherical particle is U-Mo fuel, and the black phase surrounding the U-Mo dispersed particle is matrix Al. Figure 2(b) shows irradiated fuel containing only a single-type layer in the interaction phase with virtually uniform composition throughout the interaction phase. The lines in the diffusion zones are boundaries of diffusion phase grown on the adjacent U-Mo particles. The small pores in U-Mo are fission gas bubbles. As a result of the high-temperature and high-burnup test, Al was completely consumed by the interdiffusion.

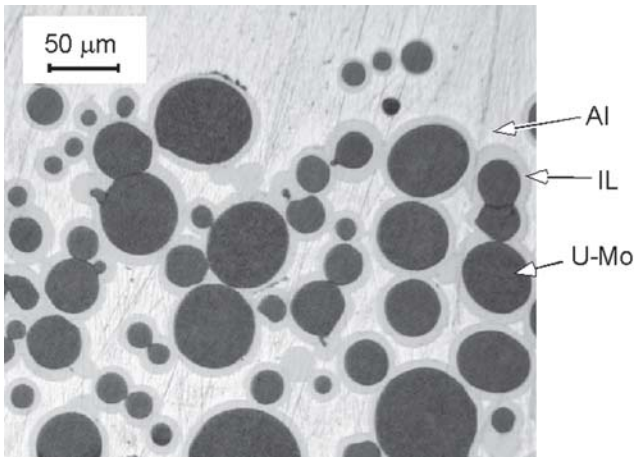

Fig. 1 Optical micrograph of U-Mo/Al dispersion fuel irradiated at ~150 °C to a burnup of 35 at.% U-235 (600D from RERTR-5 test)

The fundamental differences between out-of-pile test and in-reactor irradiation test are listed in Table 1. There is a striking contrast between the multilayer two-phase formation in the diffusion zone for out-of-pile tests and the single-layer formation for irradiation tests. The effective activa–tion energy obtained from the low-temperature regimen is 81 kJ/mol and that for the high-temperature regimen is 43 kJ/mol. The apparent change in effective activation energy with temperature is attributed to a composition change of the IL The different behavior of the diffusion zone of irradiated fuel from that of out-of-pile annealed fuel is attributed to the phenomenon of *fission-induced amorphization*. Amorphization of crystalline material by irradiation has been studied extensively in the literature.[3-7] Amorphization of a crystalline material to metallic glass is usually

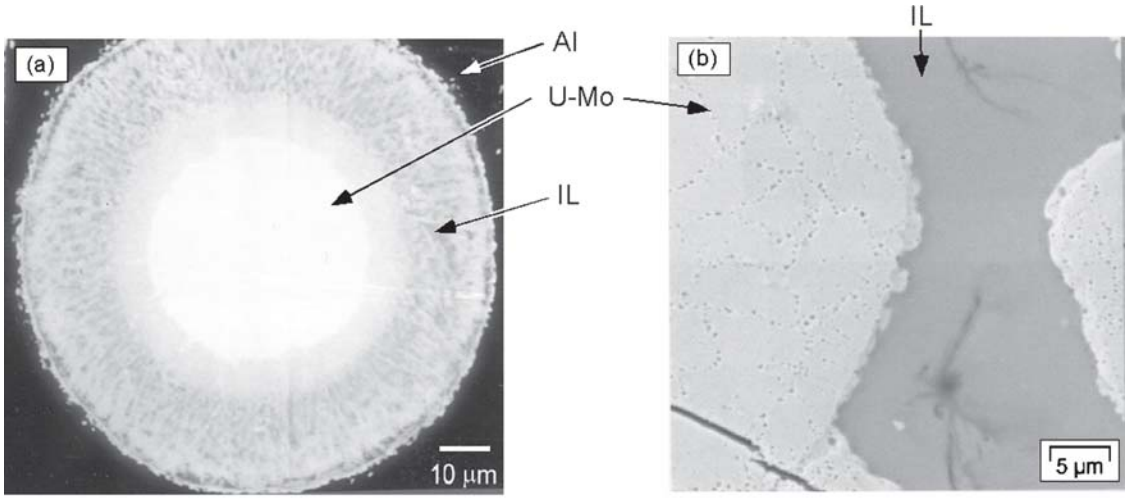

(a) SEM (BSE) of U-Mo/Al dispersion fuel heated at 525°C for 25 h [1].

(b) SEM (BSE) of U-Mo/Al from IRIS-2 at 100°C irradiated to 2.8x10^{27} fissions/m^3 (58 days) [2].

Fig. 2 Comparison of IL morphology between (a) out-of-pile test and (b) irradiation test

Table 1 Fundamental differences between out-of-pile and in-reactor tests

	Out-of-pile	In-reactor
Temperature, °C	550	<200
Time, h	<100	720 to 7200
IL morphology	Multilayers	Single layer
	Two phases per layer	Single phase with variable composition
IL structure	Crystalline	Amorphous

Table 2 Al/U + Mo) ratios of interaction products from various irradiation tests

French test	Bu, at.% U-235	Total duration, days	Maximum heat flux, W/cm^2	Clad temperature, °C	Al/(U + Mo)
IRIS-1	67	67	140	70	6-7
IRIS-2	39	40	240	105	4.4-5.8
Future	35	40	340	125	3.3-4.7
UMUS	20	48	175/250	90/110	3-4

Source: Ref 8

accompanied by an increase in volume—a quantity called "free volume" that facilitates atomic mobility, enhancing diffusion.[3] The enhancement of IL growth during irradiation can be compared with diffusion in the unrelaxed state of the metallic glass, where the so-called excess free volume associated with this unrelaxed state is dynamically maintained by the prevailing high fission rate.

Although it contained a single-layer "phase" on a fuel particle, the Al/(U + Mo) ratio of the diffusion zone of irradiated U-Mo/Al dispersion fuel was reported to have a range of $(U_{0.8}Mo_{0.2})Al_3$ to $(U_{0.8}Mo_{0.2})Al_7$, depending on the irradiation temperature, fuel loading, and burnup. An excellent data summary is available in the French RERTR program as provided in Table 2.[8] At low temperatures the Al/(U + Mo) ratio tends to be higher.

3. Diffusion Layer Growth Correlation for Out-of-Pile Tests

A measure of the extent of diffusion, for out-of-reactor data obtained by diffusion couple tests at 500 to 600 °C, is the IL thickness described by the parabolic law:

$$Y^2 = k^p t \qquad \text{(Eq 1)}$$

where Y is IL thickness, k^p is the reaction rate constant for the planar diffusion geometry given by the Arrhenius equation:

$$k^p = k_0^p \exp\left(-\frac{Q}{RT}\right) \qquad \text{(Eq 2)}$$

where k_0^p is a constant, Q is the effective activation energy, R is the gas constant, and T is temperature.

The application of the plane-surface model, however, is inappropriate to situations in which spherical particles are involved except when the layer is very thin. Rearrangement of the diffusion kinetic correlation using spherical coordinates[9] gives:

$$\frac{(\beta-1)(1-\alpha)^{2/3} + [1+(\beta-1)\alpha]^{2/3} - \beta}{2(1-\beta)} r_0^2 = k^s t \qquad \text{(Eq 3)}$$

where r_0 is the initial fuel radius, β is the ratio of the volume of product formed to the volume of fuel consumed, α is the fraction of the original fuel volume consumed, k^s is the reaction constant for the spherical geometry, and t is time. The constant α varies in the range, $0 \le \alpha \le 1$. The constant β varies depending on the product density, which is closely related to the Al/(U + Mo) ratio of the reaction product. For the diffusion products of U-Mo/Al dispersion fuel, $\beta = 3.7$ for $(U_{0.8}Mo_{0.2})Al_3$, $\beta = 4.7$ $(U_{0.8}Mo_{0.2})Al_4$, $\beta = 5.6$ for $(U_{0.8}Mo_{0.2})Al_5$, $\beta = 6.6$ for $(U_{0.8}Mo_{0.2})Al_6$, and $\beta = 7.5$ for $(U_{0.8}Mo_{0.2})Al_7$. The annealing test data used in this paper has $\beta = 3.7$ because the stoichiometry of the diffusion reaction product is $(U_{0.8}Mo_{0.2})Al_3$.[10]

The reaction constant k^s is described by the Arrhenius equation as:

$$k^s = k_0^s \exp\left(-\frac{Q}{RT}\right) \qquad \text{(Eq 4)}$$

where k_0^s is the preexponential factor and Q the effective activation energy. k_0^s and Q were obtained by using the data from the dispersion fuel annealing tests,[1,10] and the results are $k_0^s = 3.94 \times 10^{16}$ μm^2/s and $Q = 300$ kJ/mol.

The IL thickness is given by

$$Y = r_2 - r_1 \qquad \text{(Eq 5)}$$

where r_1 is the fuel radius at time t and r_2 is the radius of fuel plus the reaction product thickness at time t; that is,

$$r_1 = (1-\alpha)^{1/3} r_0 \qquad \text{(Eq 6)}$$

$$r_2 = [\beta - (\beta-1)(1-\alpha)]^{1/3} r_0 \qquad \text{(Eq 7)}$$

4. Diffusion Layer Growth Correlation for Irradiation Tests

The analytical method described in the previous section is used to fit IL thickness data measured from irradiation tests. Among the correlations, only the reaction rate constant given in Eq 4 must be changed. The reaction rate constant for irradiation test data takes the form:

$$k^i = k_0^i (F_r F_d)^{0.5} \exp\left(-\frac{Q_i}{RT}\right) \qquad \text{(Eq 8)}$$

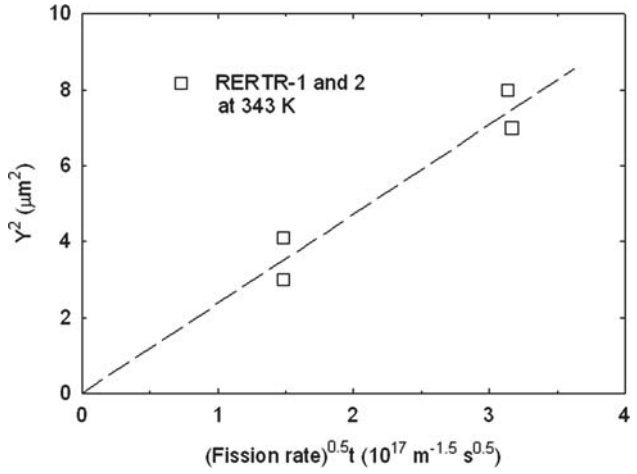

Fig. 3 Dependence of IL thickness of $(U_{0.8}Mo_{0.2})$/Al from RERTR-1 and RERTR-2 tests at fuel peak temperature ~70 °C on fission rate

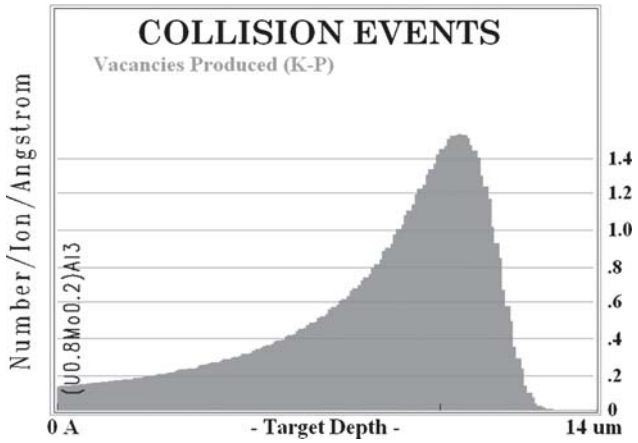

Fig. 4 TRIM result for vacancy production distribution in $(U_{0.8}Mo_{0.2})Al_3$ by 90-MeV Xe ions

where k_0^i is a constant, F_r is the fission rate in the U-Mo alloy, F_d is the fission damage factor, Q_i is the average effective activation energy during irradiation, and t is irradiation time. The correlation development processes are detailed in the subsections that follow.

The additional factors introduced from Eq 4 are F_r and F_d, accounting for irradiation enhanced diffusion. F_r is the fission rate and F_d is the damage factor, a correction factor determining the effective irradiation damage rate in the IL. Damage by only fission fragments was considered because other radiation damage such as neutron irradiation is negligible compared with that of fission fragments.[11]

The fuel fission rate is typically given by reactor physics calculations. However, the damage distribution in the diffusion zone must be evaluated. Using the TRIM code,[12] fission damage factors as a function of IL thickness were calculated for U-Mo/Al dispersion fuels. The modeling processes for the irradiation enhancement are discussed below.

4.1 Fission Density (Dose) Dependence

The IL thickness data from RERTR-1 and RERTR-2 tests are plotted as a function of the square root of fission rate multiplied by time at 343 K in Fig. 3. Y^2 shows a linear relationship with $F_r^{0.5} - t$, a quantity defined by integration of the square root of fission rate with respect to time. Although RERTR tests produced extensive irradiation data, the data applicable for this purpose were selective because the fuel temperatures changed frequently during irradiation. Therefore, only data from lower temperature tests, whose temperatures were kept fairly stable, were included in the plot.

4.2 Fission Damage Rate Dependence

Figure 4 shows an example of TRIM results for the average distribution of instantaneous vacancy production in $(U_{0.8}Mo_{0.2})Al_3$ along the direction perpendicular to the impinging surface by a fission fragment. Most of the vacancies annihilate by recombination with interstitials, leaving a small portion permanent. However, this distribution, instead of the number of vacancies, is important because it is used to obtain damage factors. As is discussed later in this section, the damage factors are normalized values. A xenon ion with the initial energy of 90 MeV was chosen to represent the average fission fragment. The range for this ion increases from 13 μm in the $(U_{0.8}Mo_{0.2})Al_3$ to 17 μm in the $(U_{0.8}Mo_{0.2})Al_6$.

Fission in the fuel is uniform so that the fission fragment generation can be modeled as point sources distributed in a square array of 0.5 μm. For the assumption of uniform distribution of fission fragment sources and the assumption of slab geometry, one-dimensional analysis is used. In other words, damage distributions by fission fragment sources on the same straight-line deposit damages on that line. Thus, the total vacancy production in the IL by the ions originating from the fuel for a given spatial point can be obtained by summing the vacancy production by ions starting from different sources 0.5 μm apart from each other. By using this scheme, the total damage rate expressed in the number of vacancies produced per angstrom IL length by fission fragments originated from the fuel is obtained as shown in Fig. 5.

Because fissile uranium is also contained in the IL, fission fragments are generated there as well. Damage created by these fission fragments is modeled similarly to the case for fission fragments from the fuel. The fission fragment sources are distributed as point sources 0.5 μm apart on the line. Because fission is isotropic, half of the ions from a source go to the right and the other half go to the left. The total damage by the ions generated in the IL at a spatial point is the sum of the damages by all ions exerted at that the point. An example for the 13 μm thick IL is shown in Fig. 6.

Because U density in the IL is lower than that of the fuel, for example, the ratio of U atom density of the $(U_{0.8}Mo_{0.2})Al_3$ to that of U-Mo fuel is 0.27, the actual fission fragment source strength in the IL is 27% of the values obtained here. By reducing the source strength this way, the total damage rate in the IL from fission fragments from the

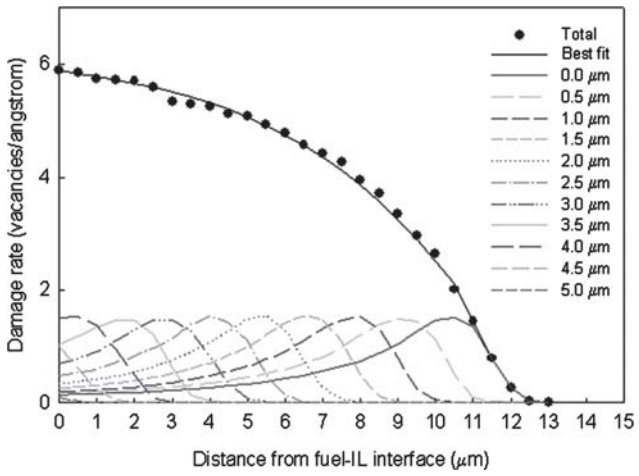

Fig. 5 Damage distribution in $(U_{0.8}Mo_{0.2})Al_3$ by 90-MeV Xe from fuel. The fuel adjoins left of the IL, and only the fission fragment (FF) flying rightward produce damage in the IL. The 0.0 μm case is for the FF starting from the fuel-IL interface. As this FF is the highest energy when it enters the IL, it leaves the longest damage track. On the other hand, the 5 μm case is for the FF produced at 5 μm from the fuel-IL interface, it leaves the shortest track.

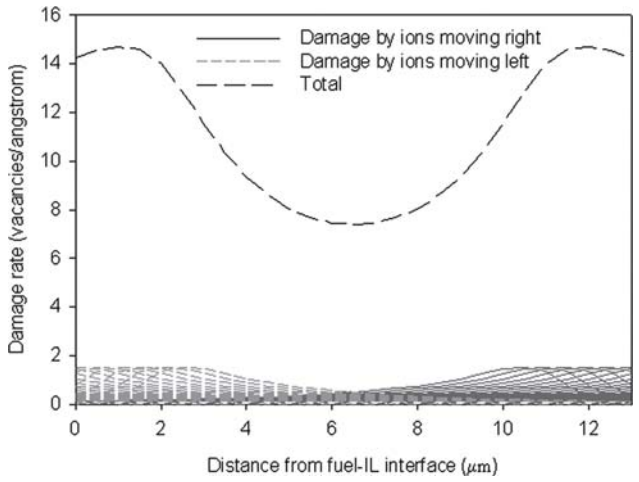

Fig. 6 Damage distribution in the 13 μm thick $(U_{0.8}Mo_{0.2})Al_3$ by fission fragments generated in the IL

fuel and IL can be obtained. The corresponding total damage rate by the fission fragments from the fuel and IL is shown in Fig. 7 as an example.

As seen in Fig. 7, interdiffusion enhancement by fission damage is lowest at the IL-Al interface due to the higher U density at the fuel-IL interface than the other side. This yields an IL with a lower Al/(U + Mo) ratio (i.e., higher in U density) at the fuel side of IL. As IL thickness increases, the rate of fission-induced Al diffusion at the IL-Al interface decreases, which may, in part, explain the observation that the overall Al/(U + Mo) ratio of an IL decreases with IL thickness. The damage rates at the fuel-IL interface for ILs with various IL thicknesses are collected and plotted in Fig. 8.

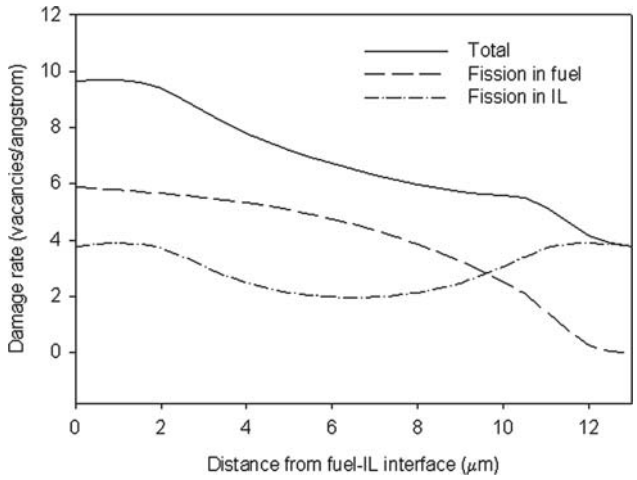

Fig. 7 Overall damage rate distribution in the 13 μm thick $(U_{0.8}Mo_{0.2})Al_3$ by ions originated both from the fuel and the IL

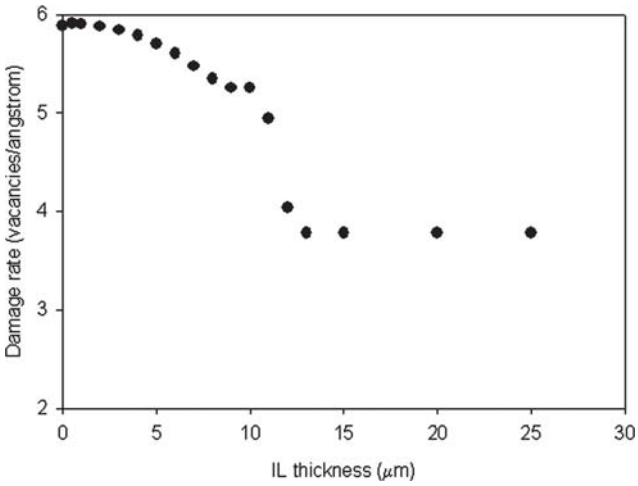

Fig. 8 Damage rate as a function of IL thickness for the IL with the composition of $(U_{0.8}Mo_{0.2})Al_3$

Following the same procedure as for the Al/(U + Mo) = 3 case, the damage rates were obtained for other IL cases with Al/(U + Mo) = 4 to 6 and normalized by the peak values of each case. The normalized values are designated as "damage factors" and are plotted in Fig. 9. Damage factors for fractional Al/(U + Mo) ratios are obtained by interpolation between the nearest integer cases. Because the density of the IL increases as the Al/(U + Mo) ratio decreases, the damage factor increases correspondingly regardless of IL thickness. On the other hand, the ion range decreases as the Al/(U + Mo) ratio decreases for the same reason.

4.3 Data Fitting

As discussed in Section 2, the composition of the IL changes depending on the irradiation temperature, fuel loading, and burnup in the range of Al/(U + Mo) = 3.3 to 7. The Al/(U + Mo) ratio of the IL was assumed to change with the fuel temperature based on data from Ref 8. The variations in

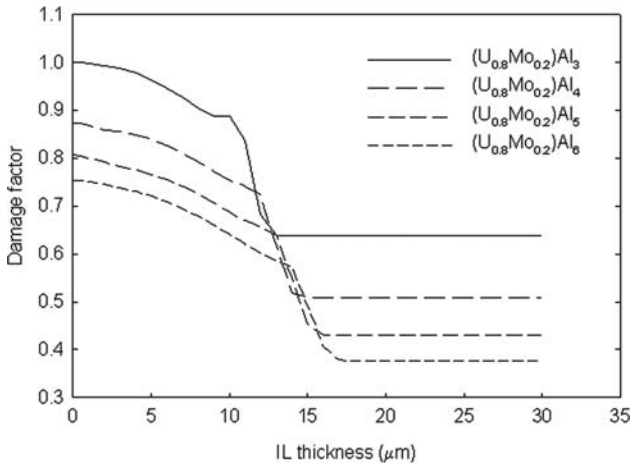

Fig. 9 Comparison of damage factors between IL cases

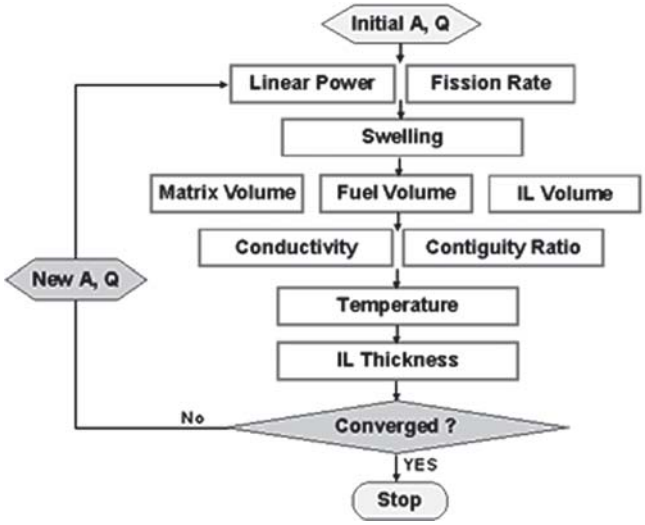

Fig. 10 Flow chart of fuel temperature and IL thickness calculation for a time

the compositions of the IL correlate with irradiation temperature. A correlation for the IL composition was obtained by matching the highest Al/(U + Mo) ratio in the data from Ref 8 to the corresponding fuel temperature, augmented 10 °C from the clad temperatures in Table 2. The lowest limit of the Al/(U + Mo) ratio, however, was set at 3.3:

$$\text{for } T \leq 443 \text{ K}, \quad x = 19.4 - 3.61 \times 10^{-2} T \qquad \text{(Eq 9a)}$$

$$\text{for } 443 \text{ K} \leq T, \quad x = 3.3 \qquad \text{(Eq 9b)}$$

where x is the Al/(U + Mo) ratio and T temperature in K. From the irradiation tests, the authors found that x always decreased irreversibly. Therefore, they used a scheme for data fitting that x remained unchanged from the previous time step for a temperature decrease and only decreased according to Eq 9 when there was a temperature increase.

The volume fraction of each phase can be calculated from the IL thickness using the ratio of the volume of the

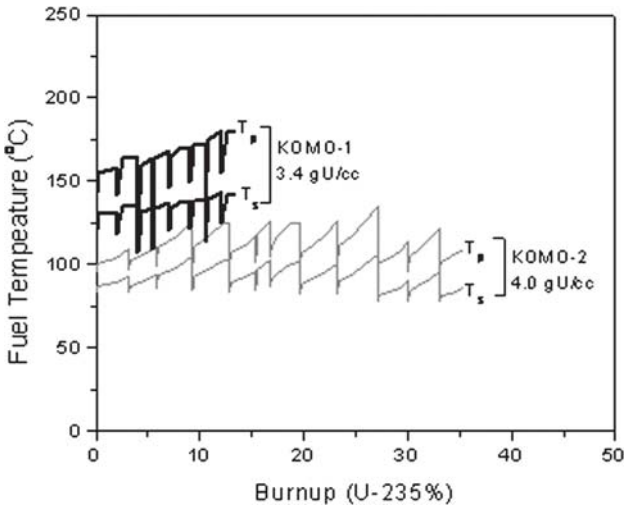

Fig. 11 Calculated temperature histories of KOMO-1 and KOMO-2 tests irradiated in the HANARO reactor at KAERI. T_p stands for the fuel peak temperature and T_s does for the fuel surface temperature. The loading of the KOMO-1 was 3.4 gU/cm^3 and that of the KOMO-2 was 4.0 gU/cm^3.

diffusion reaction product to the fuel volume, β, given in Eq 3 and the relation:

$$r_2^3 = \beta r_0^3 + (1 - \beta) r_1^3 \qquad \text{(Eq 10)}$$

where $r_1 = r_2 - Y$ is rearranged from Eq 5.

As the interaction layer grows, fuel particles begin to contact one another. To account for this situation in the quantitative analysis, the contiguity of dispersed phase was considered. The correlation for the contiguity ratio was established using measured data from RERTR irradiation tests:

$$C_F = 4.005 \times 10^{-3} V_{disp} - 3.432 \times 10^{-5} V_{disp}^2 + 9.206 \times 10^{-7} V_{disp}^3 \qquad \text{(Eq 11)}$$

where C_F is the contiguity ratio and V_{disp} is the volume fraction in percent of the dispersed phase, that is, the volume of the fuel and reaction product.

The calculation procedure to fit the correlation to the measured data is illustrated in Fig. 10. For a given fuel rod, the fuel power history is known from the reactor physics calculations. Therefore, the first step for data fitting was to divide the fueled region into four concentric rings with different thermal conductivity affected by the volume fraction of the IL. A simple time marching to the end of fuel life was used by repeating the algorithm in Fig. 10. At the end of life, the results were compared with the known measured values. If the two were different, a new set of values for the parameters, that is, the activation energy and preexponential constant, were assumed. Then, the whole process was repeated. This iteration was continued until the best fitting for all data was achieved. The same procedure was performed for other irradiated fuels. The temperature histories of the irradiated fuel rods calculated in the course of data fitting are shown in Fig. 11. The best fitting was obtained with

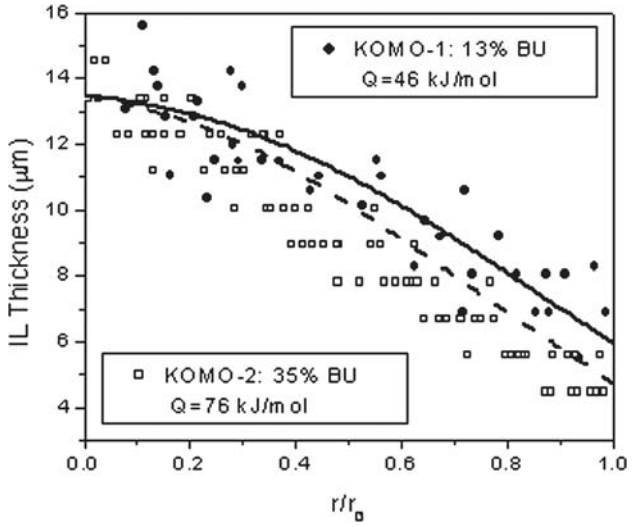

Fig. 12 Parameter fitting results compared with the KOMO-1 and KOMO-2 data

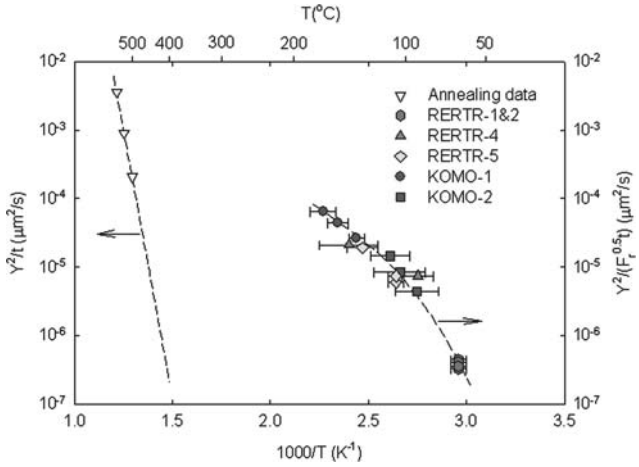

Fig. 13 Comparison of Y^2/t of out-of-pile data and $Y^2/(F_r^{0.5}t)$ of irradiation test data. The irradiation test data were divided with the square root of their fission rate factors to compare with the out-of-pile data.

Table 3 Data fitting results for KOMO-1 and KOMO-2 test data

	k_0^i, $m^{3.5}$ $s^{-0.5}$	Q_i, kJ/mol
KOMO-1	1.67×10^{-32}	46
KOMO-2	2.79×10^{-28}	76

k_0^i and Q_i values, as shown Table 3. The fitting curves are compared with the data in Fig. 12. Because the average effective activation energy was allowed to change with the fuel type to achieve the best fitting, the constant k_0^i was also changed accordingly. Horvath[13] used this method to fit the activation energy of diffusion in amorphous material.

5. Discussion

Figure 13 shows a comparison of reaction rate constants between out-of-pile annealing test data and irradiation test data from various tests. The irradiation test data were divided by the square root of the normalized fission rates to remove the fission rate effect in the plot. The average fission rate for all tests was used for normalization. The reaction rate constant for the irradiation test data is 17 orders of magnitude greater than that for the out-of-pile annealing data compared at 130 °C.

For the out-of-pile annealing test data, log (k^s) versus $1/T$ is a straight line with the slope giving the effective activation energy divided by the gas constant (Q/R). For the irradiation test data, however, the plot shows a curvature. This indicates that the average effective activation energy varied during irradiation. The effective activation energy obtained from the low-temperature regimen (i.e., for data from RERTR-1 and RERTR-2 plates and KOMO-2 fuel periphery) is 81 kJ/mol, and that from the high-temperature regimen (i.e., for data from KOMO-1 and KOMO-2 fuel center) is 43 kJ/mol. This apparent change in effective activation energy with temperature is attributed to a composition change of the IL, a change that is, among other factors, temperature dependent.

The error bars on temperature indicate the temperature variances during the tests. As the error bars show, except for low-temperature tests, the fuel temperature usually changes substantially during the test. The fuel temperatures and fission rates used in the plot are average values that vary in a nonlinear fashion during irradiation. Whereas the fission rate is calculated with a rather high accuracy and is checked with radiochemical analysis of the fuel after irradiation, the temperature calculation that involves heat transfer coefficients and, most significantly, a varying and somewhat uncertain value for the thermal conductivity, is much less accurate. It is for this reason that the growth of the IL needs to be modeled in an iterative way, and Fig. 13 should therefore be taken as an illustration of the fission-enhanced interdiffusion presented here.

Nevertheless, the fission-enhanced interdiffusion parameters obtained from the fitting procedure, namely, square-root fission rate dependence and a low activation enthalpy of 46 to 76 kJ/mol or 0.5 to 0.8 eV may be compared with, for example, ion irradiation experiments on the metallic glass $Ni_{50}Zr_{50}$ by Averback and Hahn[14] that yielded a square-root ion flux dependence and an activation enthalpy of 0.55 eV at 250 °C. The present results suggest, in analogy with the crystalline irradiation enhanced diffusion theory of Sizmann,[15] that recombination of irradiation-induced "defects" may be the underlying mechanism. The nature of these defects in an amorphous material and indeed the true mechanism of diffusion have not been conclusively resolved. The subject was very extensively reviewed by Faupel et al.[16]

The purpose of the present work was to develop an interdiffusion correlation for use in fuel behavior modeling based on fitting a plausible rate equation to measured data and calculated test parameters. The fact that the results ap-

pear to be in accordance with the current understanding of the phenomenon lends confidence to the physical meaning of the correlation.

6. Conclusions

An IL growth correlation on spherical U-Mo particles dispersed in matrix Al was obtained based on data from high-temperature annealing tests of U-Mo/Al dispersion fuel samples. The correlation has a classic Arrhenius form with a preexponential factor obtained from the best-fit, $k_0^s = 3.94 \times 10^{16}$ $\mu m^2/s$, and an effective activation energy was $Q = 300$ kJ/mol.

The reaction rate constant for irradiation tests was obtained:

$$k^i = k_0^i (F_r F_d)^{0.5} \exp\left(-\frac{Q_i}{RT}\right)$$

where Y is the IL thickness in m, k_0^i is the preexponential reaction rate constant in $m^{3.5}$ $s^{-0.5}$, F_r is the fission rate in the fuel particles in fiss/m^3-s, F_d is the unitless fission damage factor, Q_i is the average effective activation energy during irradiation in J/mol, R is the gas constant in J/mol-K, T is the fuel temperature in K, and t is the irradiation time in s. The average effective activation energy (Q_i) was best fitted with the range of 46 to 76 kJ/mol, and the corresponding preexponential factor (k_0^i) was in the range $1.67 \times 10^{-32} - 2.79 \times 10^{-28}$ $m^{3.5}$ $s^{-0.5}$, respectively.

Acknowledgment

The authors are grateful to Dr. J.M. Park and C.K. Kim for the use of the measured data collected at KAERI. This work was supported in part by the U.S. Department of Energy, Office of Global Nuclear Material Threat Reduction (NA-212), National Nuclear Security Administration, under contract W-31-109-ENG-38 and in part by the Korea Research Foundation Grant funded by the Korean Government (MOEHRD) with the grant number of KRF-2005-214-D00116.

The submitted manuscript has been created by the University of Chicago as Operator of Argonne National Laboratory (Argonne) under contract No. W-31-109-ENG-38 with the U.S. Department of Energy. The U.S. Government retains for itself, and others acting on its behalf, a paid-up, nonexclusive, irrevocable worldwide license in said article to reproduce, prepare derivative works, distribute copies to the public, and perform publicly and display publicly, by or on behalf of the Government

Argonne National Laboratory's work was supported by the U.S. Department of Energy, Office of Global Nuclear Material Threat Reduction (NA-212), national Nuclear Security Administration, under contract W-31-109-ENG-38.

References

1. H.J. Ryu, Y.S. Han, J.M. Park, S.D. Park, and C.K. Kim, Reaction Layer Growth and Reaction Heat of U-Mo/Al Dispersion Fuels Using Centrifugally Atomized Powders, *J. Nucl. Mater.,* 2003, **321,** p 210-220
2. F. Huet, J. Noirot, V. Marelle, S. Dubois, P. Boulcourt, P. Sacristan, S. Naury, and P. Lemoine, Post Irradiation Examination on UMo Full Sized Plates-IRIS2 Experiment, *Trans. Ninth International Topical Meeting on Research Reactor Fuel Management,* ENS, Budapest, Hungary, 2005, p 92-97
3. G.L. Hofman, M.R. Finlay, and Y.S. Kim, Post-Irradiation Analysis of Low Enriched U-Mo/Al Dispersions Fuel Miniplate Tests, RERTR 4 and 5, *Proc. 26th International Meeting on Reduced Enrichment for Research and Test Reactors*, Nov 7-12, 2004 (Vienna, Austria), available at www.rertr.anl.gov
4. R.M. Berman, M.L. Bleiberg, and W. Yeniscavich, Fission Fragment Damage to Crystal Structures, *J. Nucl. Mater.,* 1960, **2**(2), p 129-140
5. K. Russell, The Theory of Phase Stability under Irradiation, *J. Nucl. Mater.,* 1979, **83,** p 176-185
6. S. Klaumunzer, Ion-Beam-Induced Plastic Deformation: A Universal Phenomenon in Glasses, *Rad. Eff. Def. Sol.,* 1989, **110,** p 79-83
7. R.C. Birtcher, J.W. Richardson, and M.H. Mueller, Amorphization of U_3Si_2 by Ion or Neutron Irradiation, *J. Nucl. Mater.,* 1996, **230,** p 158-163
8. J.M. Hamy, P. Lemoine, F. Huet, B. Guigon, C. Jarousse, and J.L. Emin, Status as of March 2004 of the French UMo Group Development Program, *Trans. Eighth International Topical Meeting on Research Reactor Fuel Management,* March 21-24, 2004, ENS RRFM, Munchen, Germany, 2004
9. R.E. Carter, Kinetic Model for Solid-State Reactions, *J. Chem. Phys.,* 1961, **34**(6), p 2010-2015
10. C.K. Ho Jin Ryu, Kim, J.M. Park, Y.S. Kim, and G.L. Hofman, *Proc. TMS Conf.* (San Antonio, TX), March 12-16, 2006
11. H.J. Matzke, Radiation Enhanced Diffusion in UO_2 and $(U,Pu)O_2$, *Rad. Eff.,* 1983, **75,** p 317-325
12. J.F. Ziegler, J.P. Biersack, and U. Littmark, TRIM, 2005, available at www.SRIM.org.
13. J. Horvath, K. Pfahler, W. Ulfert, W. Frack, and H. Kronmuller, Diffusion in Amorphous Metallic Alloys, *Mater. Sci. Forum,* 1987, **15-18,** p 523-528
14. R.S. Averback and H. Hahn, Radiation-Enhanced Diffusion in Amorphous Ni-Zr alloys, *Phys. Rev.,* 1988, **B37,** p 10383-10386
15. R. Sizmann, The Effect of Radiation Upon Diffusion in Metals, *J. Nucl. Mater.,* 1978, **69-70,** p 386-412
16. F. Faupel, W. Frank, M.-P. Macht, H. Mehrer, V. Naundorf, K. Rätzke, H.R. Schober, S.K. Sharma, and H. Teichler, Diffusion in Metallic Glasses and Supercooled Melts, *Rev. Mod. Phys.,* 2003, **75,** p 237-280